ChemComm

Chemical Communications

rsc.li/chemcomm

ROYAL SOCIETY
OF **CHEMISTRY**
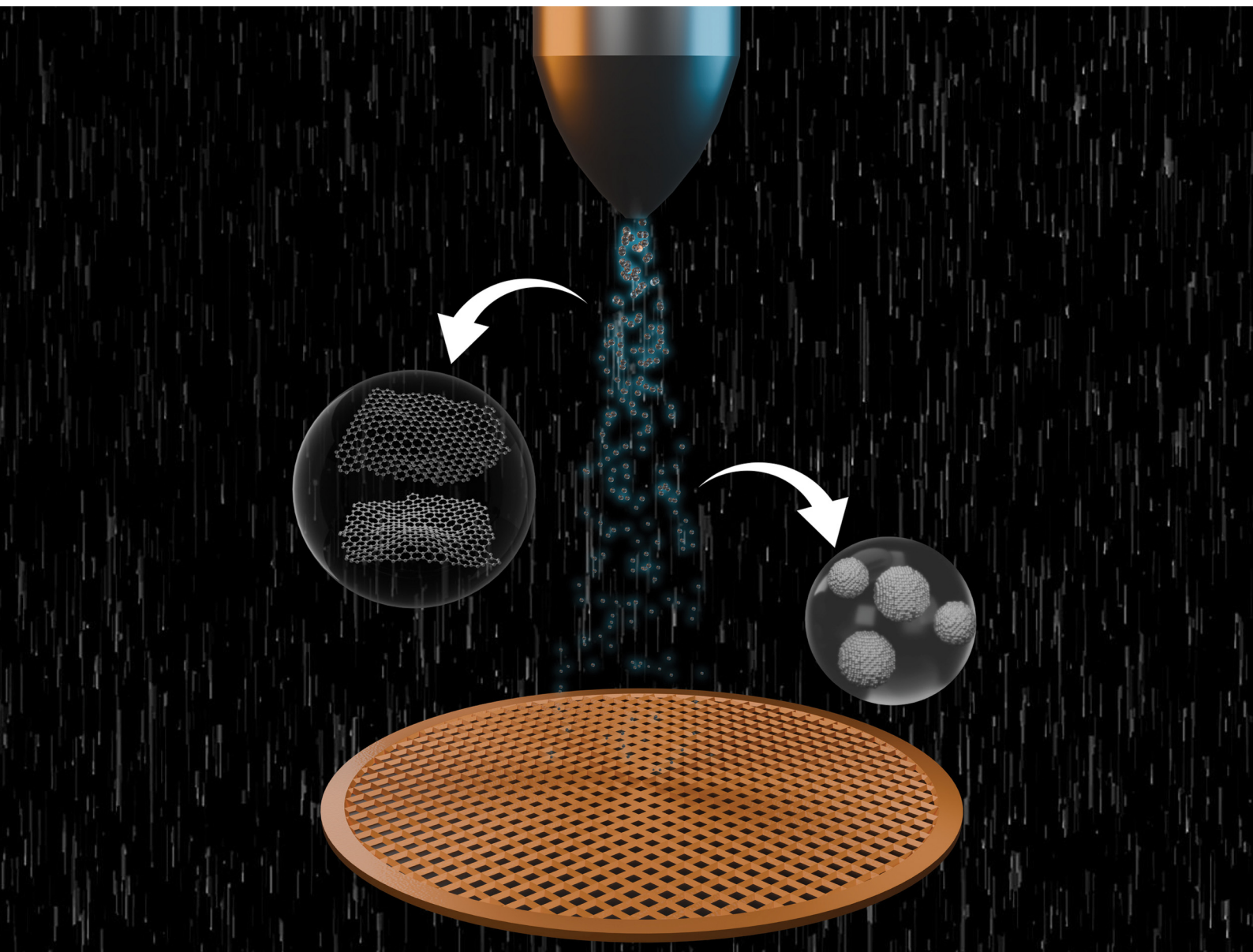
COMMUNICATION
Thalappil Pradeep *et al.*
Nanosheet-to-nanoparticle transformation in charged water
microdroplets: a pathway for 2D to 0D materials

COMMUNICATION

Check for updates

Nanosheet-to-nanoparticle transformation in charged water microdroplets: a pathway for 2D to 0D materials†

B. Krishnamurthy Spoorthi,[a] Angshuman Ray Chowdhuri,[a] Biswajit Mondal,[a] Sujan Manna,[a] Anubhav Mahapatra,[a] Amoghavarsha Ramachandra Kini[a] and Thalappil Pradeep [ID] *[ab]

This study explores the electrospray-induced transformation of molybdenum disulfide (MoS_2), graphene oxide (GO), and tungsten disulfide (WS_2) nanosheets of micrometer lateral dimensions into the respective zero-dimensional nanoparticles within the reactive environment of charged water microdroplets. The products characterized by high-resolution transmission electron microscopy (HRTEM) and Raman spectroscopy showcase charged microdroplets as an ambient, scalable medium for the synthesis of nanomaterials with promising applications in catalysis and environmental remediation.

Layered two-dimensional (2D) materials, such as MoS_2, GO, and WS_2, have attracted scientific interest due to their unique structural and electronic properties.[1–3] Their layered configuration provides a large surface area, tuneable electronic properties, and abundant edge sites, making them valuable for catalysis, sensing, and environmental applications.[4,5] The transition from the bulk to 2D enhances their reactivity and electronic characteristics, allowing them to function in ways that are not achievable in the parent form.[6] However, reducing these 2D materials to zero-dimensional (0D) structures, like nanoparticles, offers even greater benefits, including increased reactivity, due to additional quantum confinement effects, an enhanced surface-to-volume ratio, and more active sites for chemical interactions. The transformation from multilayer 2D nanosheets to 0D nanoparticles is challenging as it requires destabilizing the van der Waals forces that hold the layers together, cleavages of chemical bonds within the 2D sheets, and reproducible control of the processes leading to uniform nanoparticles. Traditional methods for achieving this transformation, such as hydrothermal processes, often demand extreme conditions, such as high energy inputs or reactive environments, which can limit

scalability and reproducibility.[7] Transformations in charged microdroplets are an innovative approach to effect the same. Electrospray produces charged microdroplets in which strong electric fields, coulombic forces, and associated effects may be used to fragment 2D nanosheets into nanoparticles under ambient conditions. Microdroplets have emerged as a unique reaction environment due to their ability to accelerate chemical reactions[8,9] and drive bond rearrangements that are not feasible in bulk solutions.[10,11] Within microdroplets, high electric fields, rapid solvent evaporation, and interfacial effects create a highly energetic microenvironment that can induce bond polarization, solvation of changes, and mechanical stress. These conditions have been shown to facilitate rapid transformations, such as oxidation, reduction, and nanoparticle assembly, occurring within micro- to milli-seconds.[12–14] The new microdroplet-based electrospray process offers a faster, safer, and more energy-efficient alternative to conventional nanoparticle synthesis. Unlike hydrothermal or chemical reduction methods, it operates under ambient conditions, avoiding high temperatures, harsh reagents, and long reaction times. Building on previous work in microdroplet-based synthesis, including our recent publication on the fragmentation of microparticles of hard minerals such as quartz and ruby into their nanoparticle analogues, *via* charged microdroplets,[15] this study focuses on the transformation of MoS_2, WS_2 and GO nanosheets into uniform nanoparticles. Using pre-prepared nanosheets simplifies transformation, as their exfoliated structure fragments easily in microdroplets. This experiment extends our understanding of microdroplet-induced transformations and explores the potential of electrospray to produce nanostructured MoS_2, GO, and WS_2 with enhanced reactivity and surface properties. By understanding how these materials behave in microdroplet environments, we can unlock new avenues for their applications in catalysis, water purification, and other environmentally focused technologies.

Briefly, to synthesize MoS_2 nanosheets, MoS_2 powder was reacted with *n*-butyllithium in hexane under argon.[16] This intercalation was followed by exfoliation in water, causing rapid H_2 evolution that separated the layers.

[a] *DST Unit of Nanoscience (DST UNS) & Thematic Unit of Excellence (TUE), Department of Chemistry, Indian Institute of Technology Madras (IITM), Chennai 600036, India. E-mail: pradeep@iitm.ac.in*

[b] *International Centre for Clean Water, 2nd Floor, B-Block, IIT Madras Research Park, Kanagam Road, Taramani, Chennai 600113, India*

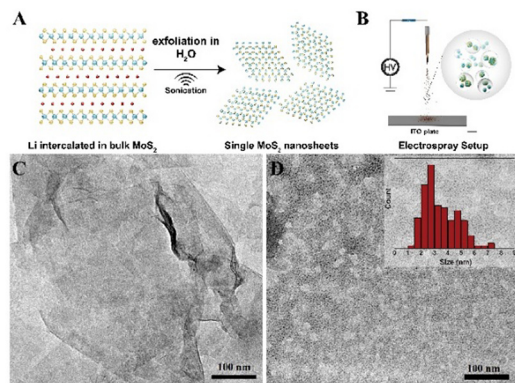† Electronic supplementary information (ESI) available. See DOI: https://doi.org/10.1039/d4cc06697a

Fig. 1 (A) A schematic of the preparation of MoS₂ nanosheets from bulk MoS₂ through wet chemical synthesis. (B) Schematic of the electrospray set-up. (C) Transmission electron microscopy (TEM) image showing the MoS₂ nanosheets synthesized by wet chemical synthesis. (D) Large area TEM image of MoS₂ nanoparticles formed by ambient electrospray. The inset shows the particle size distribution of electrosprayed MoS₂.

The nanosheets were then purified by centrifugation to isolate single- to few-layer structures (Fig. 1A). The detailed synthesis procedure is outlined in the ESI.† In this experiment, we used a custom-built nanoelectrospray source (Fig. 1B) to generate charged water microdroplets containing a fine dispersion of MoS₂ nanosheets, which were deposited onto a TEM grid positioned on an indium tin oxide (ITO)-coated collector plate. The collector was grounded *via* a picoammeter to measure the deposition current, and a voltage of approximately 3.0 kV was applied to the solution within a glass spray tip using a platinum (Pt) wire electrode. The spray plume emitted from the nanoelectrospray tip was visualized with a laser torch. Additional details of the experiment can be found in the ESI.† The electrospray setup, shown schematically in Fig. 1B, enabled the deposition of charged microdroplets containing MoS₂ nanosheets onto a substrate positioned at a defined distance from the spray tip. During deposition, a dark circular spot appeared on the substrate due to the continuous impact of the spray plume. This process led to the fragmentation of MoS₂ nanosheets into uniformly distributed nanoparticles, underscoring the role of water microdroplets and electrospray parameters in facilitating nanosheet-to-nanoparticle transformation. The nanosheets and the formed nanoparticles were examined using TEM. The TEM image of the MoS₂ nanosheets before electrospray deposition reveals a well-defined, sheet-like morphology with lateral dimensions in the nanometer range (Fig. 1C). These images show a relatively smooth and continuous surface with no observable defects, confirming the high-quality exfoliation of MoS₂ into thin nanosheets. In the TEM image of MoS₂ after electrospray (Fig. 1D), we observe a significant morphological transformation from sheet-like structures to discrete nanoparticles. The original nanosheets, characterized by their extended and layered morphology, have been effectively fragmented into uniformly distributed nanoparticles with a relatively narrow size distribution with an average size of 3.4 ± 1.5 nm (inset, Fig. 1D). These particles appear well-dispersed across the TEM grid, indicating effective breakup and dispersion, facilitated by the electrospray process (Fig. S1, ESI†). The nanoparticles

exhibit a consistent size, suggesting that the electrospray's charged microdroplets provide a controlled environment for fragmentation and stabilization. Fig. S2 (ESI†) shows the TEM images of MoS₂ nanoparticles post-electrospray at varying magnifications, indicating a clear morphological transformation. The extended and layered MoS₂ nanosheets now appear as discrete, uniformly distributed nanoparticles. The HRTEM images reveal lattice fringes with a *d*-spacing of 0.27 nm, consistent with the (100) planes of MoS₂, confirming the structural integrity of MoS₂ even after nanosheet fragmentation. This *d*-spacing further validates the transformation of MoS₂ from 2D nanosheets to well-defined 0D nanoparticle structures, retaining characteristics that are crucial for potential catalytic and electronic applications. The morphology of the nanoparticles shows spherical boundaries with minimal aggregation. The observed uniformity in particle size and shape aligns with the rapid, high-energy reactions typical of microdroplet chemistry, where transformations can occur within microseconds to milliseconds as the droplet undergoes rapid evaporation and charge-induced processes (ESI†). In the optimization of electrospray conditions, we tested a range of voltages, emitter-to-collector distances, effect of the solvent, and nebulization pressures to achieve well-dispersed MoS₂ nanoparticles. Based on trials, an optimal applied voltage of 3.0 kV was identified for an emitter-to-collector distance (*d*) of 5 mm. At this distance, uniform MoS₂ nanoparticles were observed. Water was used as a solvent to achieve the transformation. In optimizing the electrospray conditions for MoS₂ nanosheet transformation, the parameter '*d*' was varied systematically (Fig. S3, ESI†). At an optimized distance of 5 mm, uniform and well-dispersed MoS₂ nanoparticles were observed. At shorter distances (<5 mm), aggregation was evident due to limited time for the transformation, resulting in partially fragmented particles. In contrast, at longer distances (>5 mm), there was no transformation, but broken sheets were formed, likely to have been caused by changes in the electric field (ESI†). Instead of applied potential, we used varying nebulization pressures to generate microdroplets containing MoS₂ nanosheets (Fig. S5, ESI†). It is evident that the applied pressures of 10, 15, 20, and 25 psi, typically used in electrospray processes, were insufficient to induce the nanosheet-to-nanoparticle transformation and MoS₂ remained in its original nanosheet morphology. Applied voltage and the electric field strength affect the electrospray process, which can significantly influence the energy imparted to the microdroplets containing MoS₂ nanosheets, thereby affecting disintegration (Fig. S5, ESI†). For applied potentials below 3.0 kV (2.4, 2.6, and 2.8 kV), the electric field strength was insufficient to fully fragment the MoS₂ nanosheets, resulting in partial disintegration where the sheet-like morphology persisted. This limited breakdown is likely to be due to inadequate coulombic forces to overcome the interlayer interactions of the nanosheets and the bond energy within the nanosheets. At a higher potential of 3.2 kV, increased electric field strength led to particle irregularities and polydispersity, as the elevated voltage introduced instability in droplet formation. At a slightly higher potential of 3.5 kV, inorganic fullerene (IF)-like structures were observed (Fig. S6, ESI†), which suggest unique conditions within the microdroplets. In this environment, rapid

evaporation and high electric field strength promote significant structural rearrangements. The charged microdroplets are likely to have induced surface stress inducing van der Waals interactions between the MoS_2 layers, encouraging the nanosheets to bend and fold. This self-assembly process minimizes surface energy, resulting in cage-like IF structures. The electric field and confinement within microdroplets provide ideal conditions for MoS_2 to transform into these closed and stable configurations, like the formation mechanisms observed in other fullerene-like structures (ESI†). The choice of solvent greatly affects the dispersion of MoS_2 nanosheets. MoS_2 disperses well in water but tends to stack in methanol-rich environments. Testing various water-to-methanol solvent ratios (Fig. S7, ESI†) showed no disintegration of the nanosheets. Instead, increased methanol content caused the sheets to align into stacked layered structures. This stacking of MoS_2 nanosheets in methanol-rich environments is likely to be a result of methanol's lower polarity, which decreases the solubility of the MoS_2 sheets. While water provides strong dispersive forces that keep MoS_2 sheets separated, the weaker interactions of methanol allow the sheets to restack. Additionally, faster evaporation in methanol-rich droplets increases the local concentration of MoS_2, promoting aggregation. Together, these factors lead to a stacked layered structure, as van der Waals forces between sheets dominate in the less disruptive environment of methanol. The stacked sheets would need more force for fragmentation.

To explore whether GO nanosheets, a 2D material in oxide form, would undergo similar transformations to MoS_2, we electrosprayed a GO dispersion in water (details of synthesis are presented in the ESI†) at 3.5 kV. The results showed a comparable phenomenon, with the GO nanosheets transitioning into nanoparticles through ambient electrospray (Fig. 2). The initial sheet-like morphology of GO (Fig. 2A) was successfully fragmented (Fig. 2B) and formed nano-sized particles. Also, IF-like cages were observed at an applied potential of 4.0 kV (Fig. 2C and D), suggesting that the high electric field and surface stress in the electrospray environment drive self-

assembly into closed, spherical structures. These IF-like configurations in GO highlight the role of the electric field in promoting structural rearrangement, as the nanosheets fold and curve to minimize surface energy under appropriate conditions, driven by enhanced van der Waals interactions under the elevated field conditions. This process confirms that the electrospray technique can induce similar transformations in GO and MoS_2, broadening the applicability of this method to oxide-based 2D materials. To analyze the transformation of MoS_2 and GO nanosheets into nanoparticles, we conducted Raman spectroscopy of the samples collected on aluminium substrates post-electrospray (Fig. 3). The spectra provide insights into the structural and vibrational characteristics before and after transformation. The shifts in both E_{2g}^1 and A_g^1 modes reflect the transition from bulk to 2D and then to 0D forms of MoS_2 (Fig. 3A). A gradual upward shift with reduced dimensionality of the E_{2g}^1 mode (in-plane vibration) indicates layer thinning and confinement as nanoparticles.

An initial downshift with nanosheet formation, followed by an upshift in nanoparticles of the A_{1g} mode, is likely to be due to changes in out-of-plane vibrational constraints.[17–19] These changes confirm that the structural changes due to size reduction from the bulk to nanosheet to nanoparticle affect the vibrational properties of MoS_2, reflecting decreased layer interactions and increased phonon confinement in nanoparticles. Raman peaks in Fig. 3B include the D band around 1350 cm^{-1}, associated with structural defects or disorder, and the G band near 1580 cm^{-1}, which corresponds to the graphitic domains. An increase in the D/G intensity ratio after electrospray suggests enhanced disorder, consistent with the fragmentation and reorganization of GO nanosheets into nanoparticles. This observation aligns with previous findings that structural reconfiguration or reduced dimensionality can amplify defect-related signals in the Raman spectra.[20] These results confirm the effectiveness of the electrospray process in inducing transformations in both MoS_2 and GO, yielding nanoparticles that exhibit distinct structural changes observable *via* Raman peak shifts and intensity variations.

To generalize the process, we also electrosprayed WS_2, prepared similarly to the MoS_2 nanosheets as described in the ESI.† This experiment demonstrated that the transformation process is applicable to other 2D materials, following similar synthesis and electrospray conditions. As shown in
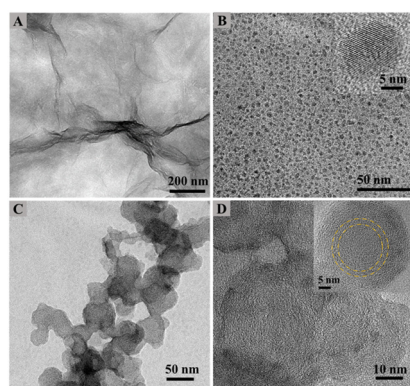
Fig. 2 Process of nanoparticle formation from GO nanosheets. (A) TEM image of the as-prepared GO nanosheet. (B) GO nanoparticles formed through ambient electrospray at 3.5 kV. (C) Formation of IF-like cages at 4.0 kV. (D) Magnified TEM images of IF-like particles. Magnification of a part of the image is presented as an inset to show the concentric stacks of GO sheets.
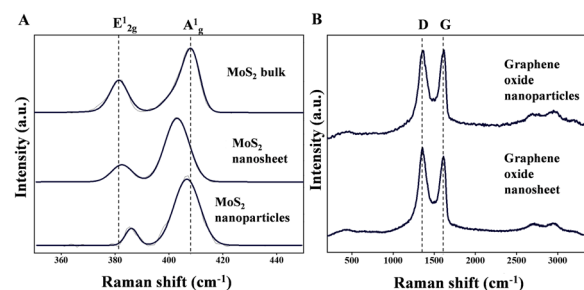
Fig. 3 Raman analysis of (A) MoS_2 bulk, nanosheets, and nanoparticles as well as (B) GO nanosheets and nanoparticles.

Fig. S8 (ESI†), WS$_2$ also underwent a structural transformation at 3.0 kV applied potential, resulting in nanoparticles with uniform morphology and crystallinity. Thus, the electrospray approach outlined is a versatile technique for converting layered 2D materials like MoS$_2$ and WS$_2$ into stable, well-dispersed nanoparticles, making it a broadly applicable method for nanoparticle synthesis across various transition metal dichalcogenides. The formation of nanoparticles from nanosheets during the electrospray process can be attributed to several contributing factors that are activated within the charged microdroplets under high electric field conditions. The key factors driving this transformation include coulombic forces, rapid solvent evaporation, confinement effects, and interlayer disruption. The high electric field polarizes the nanosheets, generating surface charges that create strong coulombic repulsion, which disrupts the interlayer van der Waals forces, promoting fragmentation (ESI†). The Coulomb explosion of the droplets results in intense pressure fluctuations within the droplets. The concentration of charges may also destabilize the layered structure enhancing interlayer separation. As the droplet shrinks, confinement within the microdroplets favors surface energy minimization, encouraging the sheets to fold or fragment into stable, spherical nanoparticles, depending on the microenvironment. This reconfiguration often leads to uniform particles or fullerene-like structures, as the nanosheets adapt to minimize energy in response to the unique electrospray conditions. As many of these effects are complex and are also further complicated by the presence of reactive species,[21–23] a consistent mechanism is yet to be developed, as in the case of mineral fragmentation.[15]

In conclusion, this study highlights the transformative potential of electrospray in synthesizing zero-dimensional nanoparticles from two-dimensional nanosheets like MoS$_2$, GO, and WS$_2$. By leveraging the unique environment of reactive microdroplets, we demonstrate a controlled and efficient pathway for nanosheet fragmentation under ambient conditions. This electrospray-based method offers a scalable, versatile alternative to conventional high-energy approaches, as shown by our TEM and Raman spectroscopy results, which reveal uniform and stable nanoparticles with enhanced reactivity and structural integrity. These findings underscore the promise of the electrospray method for advancing nanomaterials synthesis, with potential applications in catalysis, environmental remediation, and beyond. This work opens doors to novel applications of microdroplet chemistry in nanotechnology, emphasizing the role of ambient electrospray in precision fabrication with sustainability. However, it needs further validation across additional materials.

Data availability

The data supporting this article, including all experimental results and analysis, are included in the main article and its ESI.† No additional data have been deposited in external repositories.

Conflicts of interest

There are no conflicts to declare.

Notes and references

1 W. Zhao, R. M. Ribeiro and G. Eda, *Acc. Chem. Res.*, 2015, **48**, 91–99.
2 W. Zhao, J. Pan, Y. Fang, X. Che, D. Wang, K. Bu and F. Huang, *Chem. – Eur. J.*, 2018, **24**, 15942–15954.
3 X. Li, L. Tao, Z. Chen, H. Fang, X. Li, X. Wang, J. Bin Xu and H. Zhu, *Appl. Phys. Rev.*, 2017, **4**, 021306.
4 Z. Wang and B. Mi, *Environ. Sci. Technol.*, 2017, **51**, 8229–8244.
5 B. L. Li, M. I. Setyawati, H. L. Zou, J. X. Dong, H. Q. Luo, N. B. Li and D. T. Leong, *Small*, 2017, **13**, 1–20.
6 M. Chhowalla, H. S. Shin, G. Eda, L. J. Li, K. P. Loh and H. Zhang, *Nat. Chem.*, 2013, **5**, 263–275.
7 D. Pan, J. Zhang, Z. Li and M. Wu, *Adv. Mater.*, 2010, **22**, 734–738.
8 S. Banerjee and R. N. Zare, *Angew. Chem., Int. Ed.*, 2015, **54**, 14795–14799.
9 K. Naveen, V. S. Rawat, R. Verma and E. Gnanamani, *Chem. Commun.*, 2024, **60**, 13263–13266.
10 Z. Wei, Y. Li, R. G. Cooks and X. Yan, *Annu. Rev. Phys. Chem.*, 2020, **71**, 31–51.
11 S. Bose, M. Mofidfar and R. N. Zare, *J. Am. Chem. Soc.*, 2024, **146**, 27964–27971.
12 J. K. Lee, K. L. Walker, H. S. Han, J. Kang, F. B. Prinz, R. M. Waymouth, H. G. Nam and R. N. Zare, *Proc. Natl. Acad. Sci. U. S. A.*, 2019, **116**, 19294–19298.
13 C. Gong, D. Li, X. Li, D. Zhang, D. Xing, L. Zhao, X. Yuan and X. Zhang, *J. Am. Chem. Soc.*, 2022, **144**, 3510–3516.
14 A. Ray Chowdhuri, B. K. Spoorthi, B. Mondal, P. Bose, S. Bose and T. Pradeep, *Chem. Sci.*, 2021, **12**, 6370–6377.
15 B. K. Spoorthi, K. Debnath, P. Basuri, A. Nagar, U. V. Waghmare and T. Pradeep, *Science*, 2024, **384**, 1012–1017.
16 L. Yuwen, H. Yu, X. Yang, J. Zhou, Q. Zhang, Y. Zhang, Z. Luo, S. Su and L. Wang, *Chem. Commun.*, 2016, **52**, 529–532.
17 X. Zhang, W. P. Han, J. B. Wu, S. Milana, Y. Lu, Q. Q. Li, A. C. Ferrari and P. H. Tan, *Phys. Rev. B: Condens. Matter Mater. Phys.*, 2013, **87**, 1–8.
18 A. Berkdemir, H. R. Gutiérrez, A. R. Botello-Méndez, N. Perea-López, A. L. Elías, C. I. Chia, B. Wang, V. H. Crespi, F. López-Urías, J. C. Charlier, H. Terrones and M. Terrones, *Sci. Rep.*, 2013, **3**, 1–8.
19 C. Lee, H. Yan, L. E. Brus, T. F. Heinz, J. Hone and S. Ryu, *ACS Nano*, 2010, **4**, 2695–2700.
20 Å. Björkman, *Schweiz. Z. Hydrol.*, 1969, **31**, 632–645.
21 M. Angelaki, J. D'Erceville, D. J. Donaldson and C. George, *J. Am. Chem. Soc.*, 2024, 2–6.
22 D. Xing, Y. Meng, X. Yuan, S. Jin, X. Song, R. N. Zare and X. Zhang, *Angew. Chem., Int. Ed.*, 2022, **61**, e202207587.
23 L. E. Krushinski and J. E. Dick, *Proc. Natl. Acad. Sci. U. S. A.*, 2024, **121**, e2321064121.